Journal Pre-proof

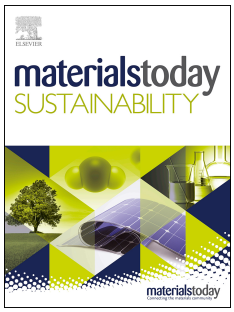

The mechanism of hydride formation during electrochemical hydrogen charging of Ti-6Al-4V

L. Deconinck, T Depover, K. Verbeken

PII: S2589-2347(23)00073-8

DOI: https://doi.org/10.1016/j.mtsust.2023.100387

Reference: MTSUST 100387

To appear in: *Materials Today Sustainability*

Received Date: 9 November 2022

Revised Date: 13 February 2023

Accepted Date: 16 March 2023

Please cite this article as: L. Deconinck, T Depover, K. Verbeken, The mechanism of hydride formation during electrochemical hydrogen charging of Ti-6Al-4V, *Materials Today Sustainability*, https://doi.org/10.1016/j.mtsust.2023.100387.

The mechanism of hydride formation during electrochemical hydrogen charging of Ti-6Al-4V

Authors: L. Deconinck, T. Depover*, K. Verbeken*

CRediT author statement

L. Deconinck:
Conceptualisation, Methodology, Validation, Investigation, Formal analysis, Visualisation, Writing – original draft.

T. Depover:
Conceptualisation, Methodology, Writing – Review & Editing, Supervision, Project administration, Funding acquisition.

K. Verbeken:
Methodology, Writing – Review & Editing, Supervision, Project administration, Funding acquisition

Hydride formation mechanism at room temperature

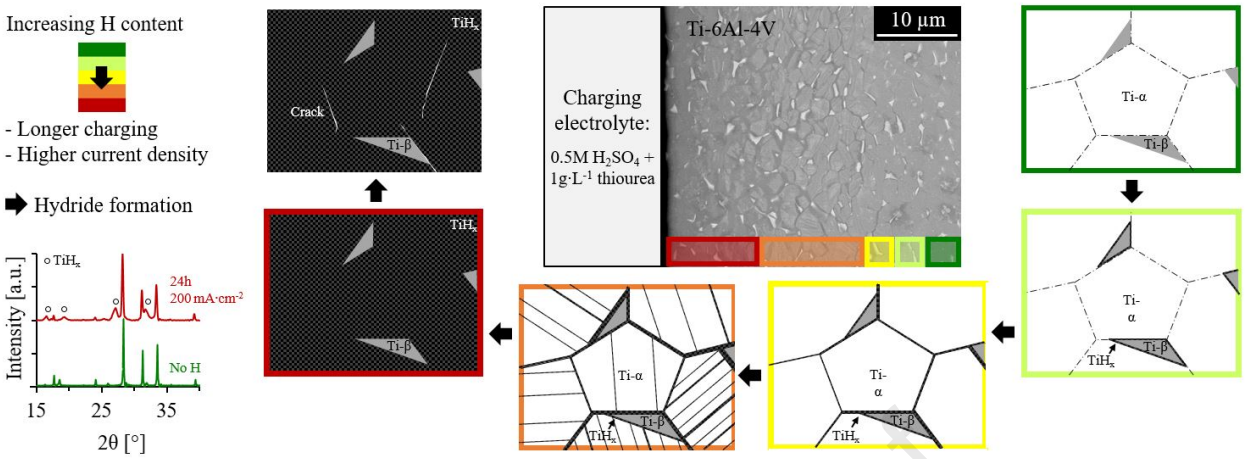

The mechanism of hydride formation during electrochemical hydrogen charging of Ti-6Al-4V

Authors: L. Deconinck, T. Depover*, K. Verbeken*

Ghent University, Department of Materials, Textiles and Chemical Engineering, Research Group of Sustainable Materials Science, Technologiepark 46, 9052 Ghent, Belgium

* Corresponding authors

E-mail addresses: Liesbet.Deconinck@UGent.be (L. Deconinck), Tom.Depover@UGent.be (T. Depover), Kim.Verbeken@UGent.be (K. Verbeken)

Keywords: Ti-6Al-4V; electrochemical hydrogen charging; diffusion; titanium hydride formation; phase transformation

Abstract

The present work studies experimentally the hydrogen uptake and hydride formation in duplex Ti-6Al-4V. Hydrogen is introduced by electrochemical hydrogen charging at room temperature. The effect of the applied charging conditions is evaluated considering the effect of charging duration and charging current density. Moderate charging conditions induce solute hydrogen in the lattice, resulting in lattice strains, as revealed by X-ray diffraction. More severe hydrogen exposure results in the formation of titanium hydrides when the hydrogen concentration exceeds the solubility limit of the Ti-α phase, as verified by a combined characterisation with X-ray diffraction, scanning electron microscopy, electron backscatter diffraction, and hydrogen melt extraction. A progressive mechanism of hydride formation upon increasing hydrogen content is proposed as the charging conditions clearly influence hydrogen distribution and hydride formation in the material. Controlling the electrochemical hydrogen charging conditions enables to further understand the role of hydrogen and hydrides in hydrogen induced failure mechanisms, as well as it offers opportunities for sustainable thermohydrogen processing of titanium.

1. Introduction: interaction between hydrogen and titanium

The titanium alloy Ti-6Al-4V is the workhorse of the titanium industry, possessing a high specific strength, good mechanical characteristics and an excellent corrosion resistance [1]. This unique combination of properties is among others applied in high-end applications in the aerospace, offshore and biomedical industry [2]. Titanium's large oxygen affinity results in a stable and adherent oxide layer, which provides a good corrosion protection in various environments [3]. Besides, titanium also has a high affinity to hydrogen and is able to absorb large amounts of hydrogen [4]. Upon high hydrogen concentration, titanium hydrides form [2]. The titanium hydride phase shows application potential due to the reversible hydrogen sorption reaction [5]. Titanium hydrogenation is for example applied in thermohydrogen processing where hydrogen is used as a temporary alloying element. Since hydrogen is easily added and removed in titanium without melting, it can contribute to refine the microstructure, improve the processability and enhance mechanical properties [6]. However, the brittle hydride phase could also be associated with detrimental effects since titanium hydrides facilitate material degradation, according to the failure mechanism of hydride induced degradation [7]. Therefore, profound understanding on the development of titanium hydrides at room temperature is required.

The Ti-6Al-4V microstructure consists of a hexagonally close packed α phase and a body centred cubic β phase. Aluminium is in charge of stabilising the Ti-α phase, whereas vanadium stabilises the Ti-β phase at room temperature. However, the hydrogen uptake and diffusion characteristics significantly differ for these phases [3, 8–10]. The hydrogen diffusivity in Ti-α and Ti-β obeys an Arrhenius equation, with a temperature dependence and a corresponding activation energy. At room temperature, the diffusion rate differs several orders of magnitude in D_α (ranging between $3.26 \cdot 10^{-17}$ $m^2 \cdot s^{-1}$ and $1.05 \cdot 10^{-15}$ $m^2 \cdot s^{-1}$) compared to D_β (in the range of $2.17 \cdot 10^{-12}$ $m^2 \cdot s^{-1}$ to $2.32 \cdot 10^{-11}$ $m^2 \cdot s^{-1}$) according to [7, 11]. Therefore, in α-β titanium alloys such as Ti-6Al-4V, the Ti-β phase is often considered as a highway for

hydrogen transport as presented in [12]. The relative amount and distribution of the α-phase and β-phase determine the hydrogen transport path, as shown by Tal-Gutelmacher et al. [13]. Furthermore, the terminal hydrogen solubility in Ti-α ($2 \cdot 10^3$ wppm) is lower than the solubility in Ti-β ($20.6 \cdot 10^3$ wppm) following Baker in [14]. Therefore, the Ti-β phase is considered as a hydrogen reservoir [7]. Furthermore, hydrogen has a stabilising effect on the Ti-β phase, resulting in a decrease of the α-to-β transition temperature [12]. Moreover, titanium hydrides form upon exceeding the hydrogen solubility limit. Typical orientation relationships have been reported for preferential hydride precipitation with respect to the Ti-α phase [15, 16]. The titanium hydride crystal structure depends on the stoichiometric formula. At room temperature, the metastable γ-TiH_x ($x<1.5$) consists of a face centred tetragonal (fct) crystal lattice with $c/a>1$, while δ-TiH_x ($1.5<x<1.99$) has a face centred cubic (fcc) lattice, which transforms diffusionless upon increasing hydrogen content to fct ε-TiH_x ($x>1.99$) with $c/a<1$ [12]. Furthermore, the transformation to the TiH_x hydride phase caused a volume increase of 18% in Ti-α and 5.35% in Ti-β, according to [7]. Additionally, the hydrogen diffusion in titanium hydride was discussed to be 10^{-14} $m^2 \cdot s^{-1}$ by Ivasishin et al. [17], whereas Wipf et al. [18] reported values in the range of 10^{-16} $m^2 \cdot s^{-1}$ in δ-hydride at room temperature.

Research on titanium hydrogenation is often performed by gaseous hydrogen charging at elevated temperatures [13, 19–21]. The hydrogen characteristics in the microstructure are well understood under these conditions for the purpose of thermohydrogen processing [6, 22]. For such low hydrogen fugacity by gaseous charging at higher temperatures, the mechanism of hydride formation was described using hydrogen diffusion models in [11, 23] and [24] as well as by martensitic phase transformations in [25]. Martensitic Ti-α' forms upon cooling and plays hereby an initiating role in the hydride formation process [23]. Nevertheless, for high hydrogen fugacity in electrochemical charging at room temperature, no martensitic phase nor cooling-related phase transformations are present. Therefore, in order to overcome the limited knowledge on room temperature hydrogen charging, this work aims to determine a mechanism for hydride formation at high hydrogen fugacity. The role of electrochemical charging parameters, i.e. charging duration and charging current density, were investigated. The hydrogen uptake and hydride formation in the Ti-6Al-4V alloy were characterised by X-ray diffraction (XRD), scanning electron microscopy (SEM), electron backscatter diffraction (EBSD), and hydrogen melt extraction.

2. Materials and methods

A commercial Ti-6Al-4V sheet from TiPro was used in this work. The material was cold rolled to 1 mm thickness, meeting ASTM B265 [26]. The material was homogeneous throughout the complete plate. The chemical composition is presented in Table 1.

Table 1: Chemical composition of titanium grade 5 (Ti-6Al-4V) [26]

Grade 5	**Al**	**V**	**Fe**	**O**	**C**	**N**	**H**	**Ti**
[wt%]	5.5-6.75	3.5-4.5	< 0.4	< 0.2	< 0.08	< 0.05	< 0.015	Balance

Since the investigated phenomena of hydrogen diffusion and subsequent hydride formation occurred slowly during the applied galvanostatic hydrogen charging, the sample's cross section was considered in order to allow investigation of the evolution of titanium hydride formation. All cross sections were taken as presented in Figure 1. After electrochemical hydrogen charging, the specimen was transversally cut with subsequent grinding and polishing for further microscopic examination. All specimens underwent metallographic grinding according to the standard techniques, followed by rough polishing with a 9 µm diamond suspension. Fine polishing occurred with a fresh solution of 70 vol% colloidal silica suspension OP-S and 30 vol% H_2O_2 (35 wt%). Microstructural analysis was performed by a FEI Quanta 450 with field emission gun for scanning electron microscopy (SEM), using the backscatter electron (BSE) detector at an accelerating voltage of 20 kV and a spot size of 5. Electron backscatter diffraction (EBSD) was carried out on the same device, using a tilt angle of 70° and a hexagonal grid

base. Post-processing was done with the TSL-OIM Data Analysis software. Points with a confidence index below 0.1 were not considered and remained black in the analysis.

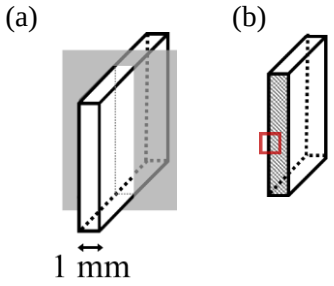

Figure 1: Schematic representation of cross sections taken in the hydrogen charged samples. (a) Cutting plane, indicated in grey. (b) Imaging plane after polishing the cross section. In the microscopic imaging in this work, the specimen's surface is always depicted at the left side, whereas more to the right of the image represents deeper into the bulk. The red square shows an example of the imaged area.

Additionally, X-ray diffraction measurements were performed to identify the present phases, in particular to confirm the appearance of titanium hydrides. A Siemens Kristalloflex D5000 diffractometer was used with a Mo-Kα-source, operating at 40 mA and 40 kV. The angle 2θ ranged from 15° to 40° with 0.008° step size and 5 s holding time per step.

The effect of the hydrogen presence was investigated by introducing hydrogen via electrochemical charging at room temperature. Therefore, the specimen acted as cathode for hydrogen evolution, while two neighbouring platina foils served as anode. The electrolyte consisted of a 0.5 M H_2SO_4 solution with 1 $g \cdot L^{-1}$ thiourea. Thiourea was added to promote atomic hydrogen absorption into the metal, since it poisons the hydrogen recombination reaction to the molecular H_2 form. Galvanostatic charging was applied using different constant current densities, i.e. 0.8 $mA \cdot cm^{-2}$, 50 $mA \cdot cm^{-2}$, 100 $mA \cdot cm^{-2}$ and 200 $mA \cdot cm^{-2}$. Moreover, the charging duration was varied as well, including one day, one week, two weeks and three weeks. As such, the role of applied current density and charging duration could be evaluated in a systematic approach. The associated potential remained well under the corrosion potential during the course of the experiments. The specimen's surface and edges were ground to grit size 1200 before the charging procedure. The hydrogen uptake capacity was determined by melt extraction with a Bruker Galileo G8. A thermal conductivity detector measured the released hydrogen at 1600°C, following the conductivity difference between the liberated H_2 gas and the N_2 carrier gas. Each charging condition was analysed at least in threefold. The specimen's dimensions were 10 mm x 5 mm x 0.4 mm.

3. Results

The microstructure of uncharged Ti-6Al-4V was determined by SEM-BSE microscopy, as presented in Figure 2. The considered alloy with duplex structure consisted of 91.5 vol% Ti-α phase with 8.5 vol% uniformly distributed Ti-β islands. The grains were flattened in the normal direction owing to the rolling production process, whereas they were slightly elongated in the transversal and even more in the rolling direction. The Ti-β phase was not interconnected in this duplex microstructure. Therefore, the Ti-β phase will not enable a short-circuiting transport path for hydrogen, as opposed to the findings presented in [12] where Ti-β formed a connected network. Nevertheless, the Ti-β phase is still assumed to be able to act as hydrogen storage tank due to the significantly larger hydrogen solubility in Ti-β compared to Ti-α.

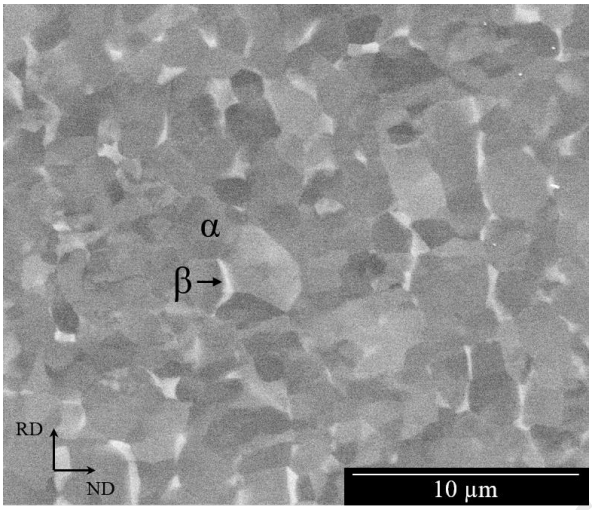

Figure 2: SEM-BSE micrograph of the microstructure of uncharged duplex Ti-6Al-4V with brighter contrast Ti-β grains in the grey contrast Ti-α matrix. Overall, the considered alloy consisted of 91.5 vol% Ti-α phase with 8.5 vol% islands of Ti-β phase.

In order to evaluate the hydrogen evolution and hydride formation process, two main charging parameters were varied, i.e. charging duration and charging current density. The corresponding total hydrogen content was determined by melt extraction for the different applied charging conditions. The results are presented in Figure 3. The hydrogen content increased both upon increasing charging duration and increasing current density. High current density charging for a short period, introduced more hydrogen compared to low current density charging for a longer period. The global quantity of hydrogen introduced did not reach the hydrogen solubility limit as defined in [14]. Meanwhile, the hydrogen content continuously increased with increasing hydrogen charging. Therefore, specimen saturation was not yet achieved by the applied hydrogen charging conditions due to the low diffusion coefficient of hydrogen in titanium. Furthermore, hydrogen was already present in the uncharged reference specimens as a result of the production process.

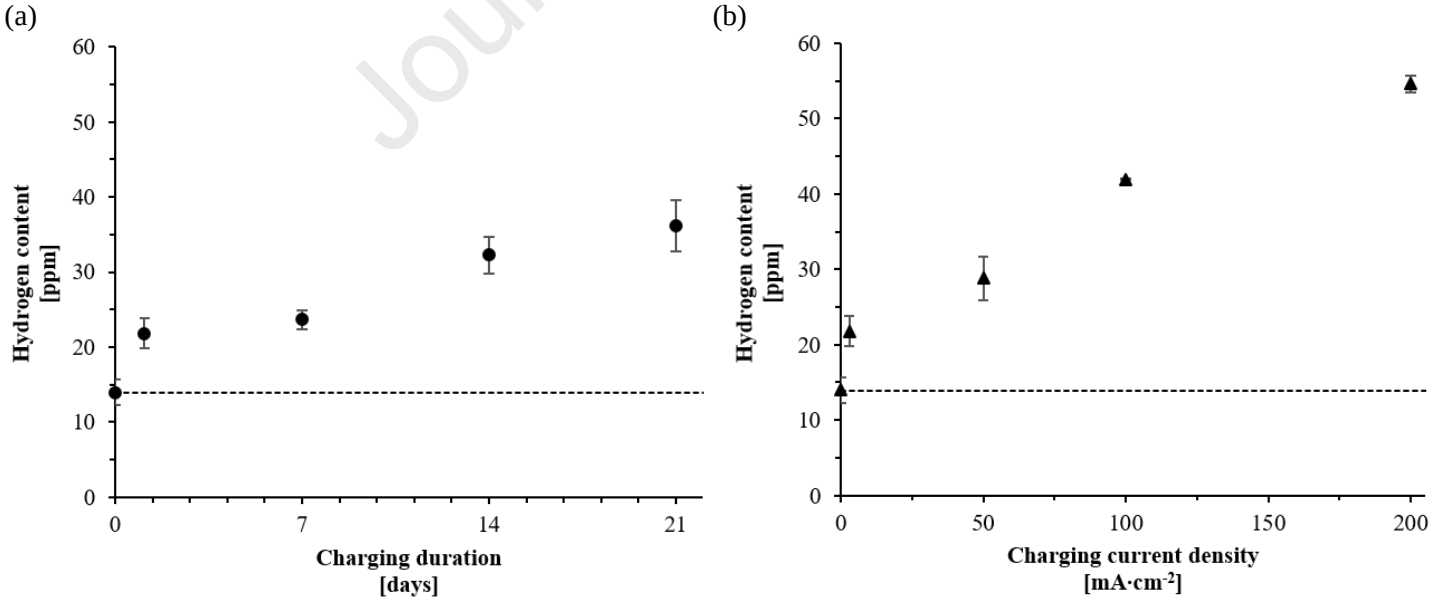

Figure 3: Total hydrogen concentration based on melt extraction of electrochemically charged Ti-6Al-4V. Each condition was measured in threefold. The dashed line represents the hydrogen content present in uncharged reference specimens. (a) Variable charging duration at 0.8 mA·cm^{-2} constant current density. (b) Variable charging current density charged for one day.

Additionally, X-ray diffraction was used to verify whether hydrides had formed by the applied charging conditions. Figure 4 shows the characteristic XRD peaks corresponding to increasing hydrogen charging duration and charging current density. At low charging current density (Figure 4a), only Ti-α and Ti-β peaks were visible, even for longer charging durations. At higher current density (Figure 4b), characteristic titanium hydride peaks appeared after one day, being more intense for higher charging current densities. Ti-α and Ti-β peaks were still present as well in the spectrum after high current density charging. Therefore, the hydrides did not take over the total microstructure as was observed in XRD spectra of high hydrogen fugacity electrochemical charging of commercially pure titanium (consisting only of Ti-α) [27]. The hydride peaks were all located at characteristic positions corresponding to the γ-hydride type [28]. Furthermore, the introduced titanium hydrides were stable at room temperature. However, these hydride peaks disappeared from the XRD spectrum when heating above 700°C, which was assumed to be above the hydrogen desorption temperature and far above the titanium hydride dissociation temperature [29, 30].

For both charging parameters, i.e. long duration charging and high current density charging, a slight peak shift to the left as well as modest peak broadening was visible with respect to the uncharged condition, which indicated an increase in lattice constant and internal strain, respectively. The introduced solute hydrogen was responsible for this increase in lattice strain. The corresponding lattice parameters are quantified in Table 2. These values demonstrated that the lattice strains were barely present in the Ti-β phase since the measured Ti-β lattice spacing remained relatively constant upon severe charging. Also lattice parameter *'a'* in the Ti-α phase did not significantly change with variation of charging parameter. Contrarily, lattice parameter *'c'* in the Ti-α phase increased upon more intense hydrogen charging. As a comparison from literature, Tal-Gutelmacher and Eliezer [12] reported that the lattice parameter '*a*' of the TiH_2 phase ranged between 4.23 and 4.54 Å after 69 hours electrochemical charging at 50 $mA \cdot cm^{-1}$ in a glycerol-phosphoric acid electrolyte.

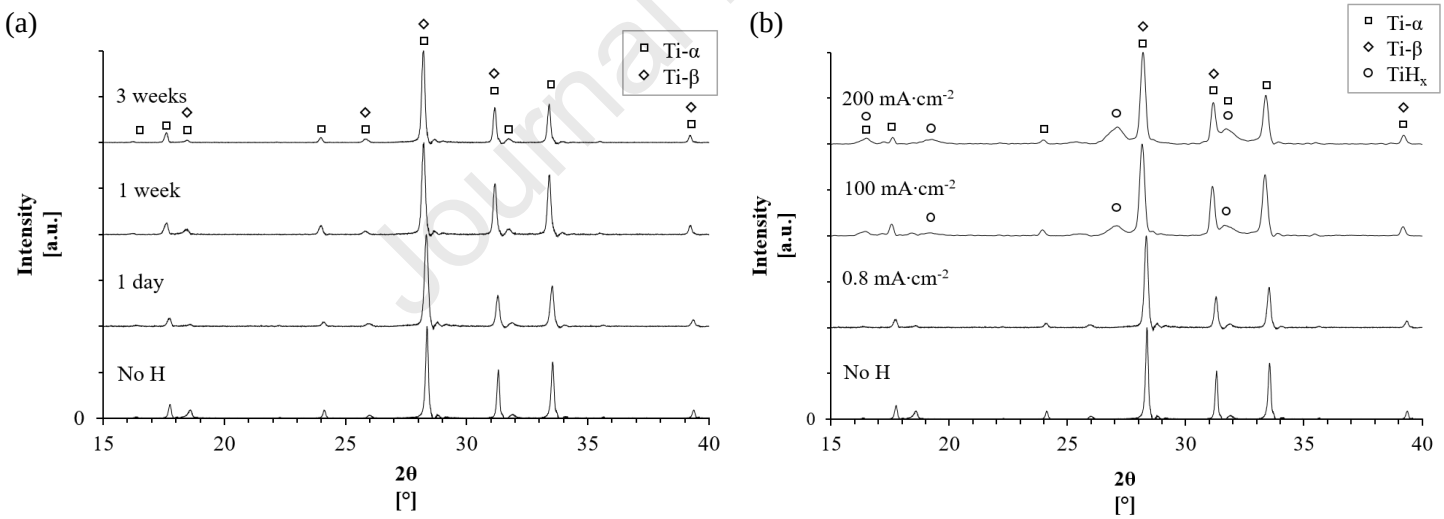

Figure 4: XRD spectra of electrochemically hydrogen charged Ti-6Al-4V with (a) variable charging duration at 0.8 $mA \cdot cm^{-2}$ and (b) one day charging at variable current density. The observed peak shift and peak broadening indicated the presence of lattice strains due to interstitial hydrogen. Titanium hydride peaks appeared upon more severe charging current densities.

Table 2: Crystal lattice parameters of uncharged and electrochemically hydrogen charged Ti-6Al-4V from XRD peak positions. The lattice spacing increased upon more severe hydrogen charging in the Ti-α phase.

Phase	**Ti-α**		**Ti-β**
Lattice parameter	**a [Å]**	**c [Å]**	**a [Å]**
Uncharged	2.85 ± 0.06	4.61 ± 0.05	3.20 ± 0.03
1 day 0.8 mA·cm^{-2}	2.85 ± 0.05	4.62 ± 0.03	3.19 ± 0.04
3 weeks 0.8 mA·cm^{-2}	2.86 ± 0.04	4.68 ± 0.03	3.18 ± 0.02
1 day 200 mA·cm^{-2}	2.87 ± 0.04	4.69 ± 0.03	3.21 ± 0.05

Complementary SEM-BSE micrographs revealed microstructural characteristics of the titanium hydrides. Figure 5 shows the cross section (conform to Figure 1) of multiple hydrogen charged specimens under various constant charging conditions at room temperature. Upon more severe hydrogen charging conditions, a darker grey hue progressively appeared along phase and grain boundaries, which was consistent along the complete edge side. Based on the appearance of the hydride peaks during X-ray diffraction measurements, this dark grey contrast represents the titanium hydride phase. The introduced hydrogen was heterogeneously distributed over the thickness of the sample due to the high fugacity charging method and the slow diffusion rate of hydrogen in titanium. As a result, titanium hydrides did form near the sample's edge as the hydrogen solubility limit was locally exceeded there. Based on these micrographs, a mechanism of hydride formation for high fugacity hydrogen charging at room temperature is proposed below. Moreover, although hydride traces were visible in Figure 5c for long charging times at low current density, the quantity of titanium hydrides was not sufficient to be detected by XRD, taking into account the interaction volume of the technique since it provides information on the outer tens of microns underneath the surface [31]. Furthermore, considering that interaction volume, these micrographs explain why Ti-α and Ti-β peaks were still prominently present in the XRD spectra of high current density charged specimens.

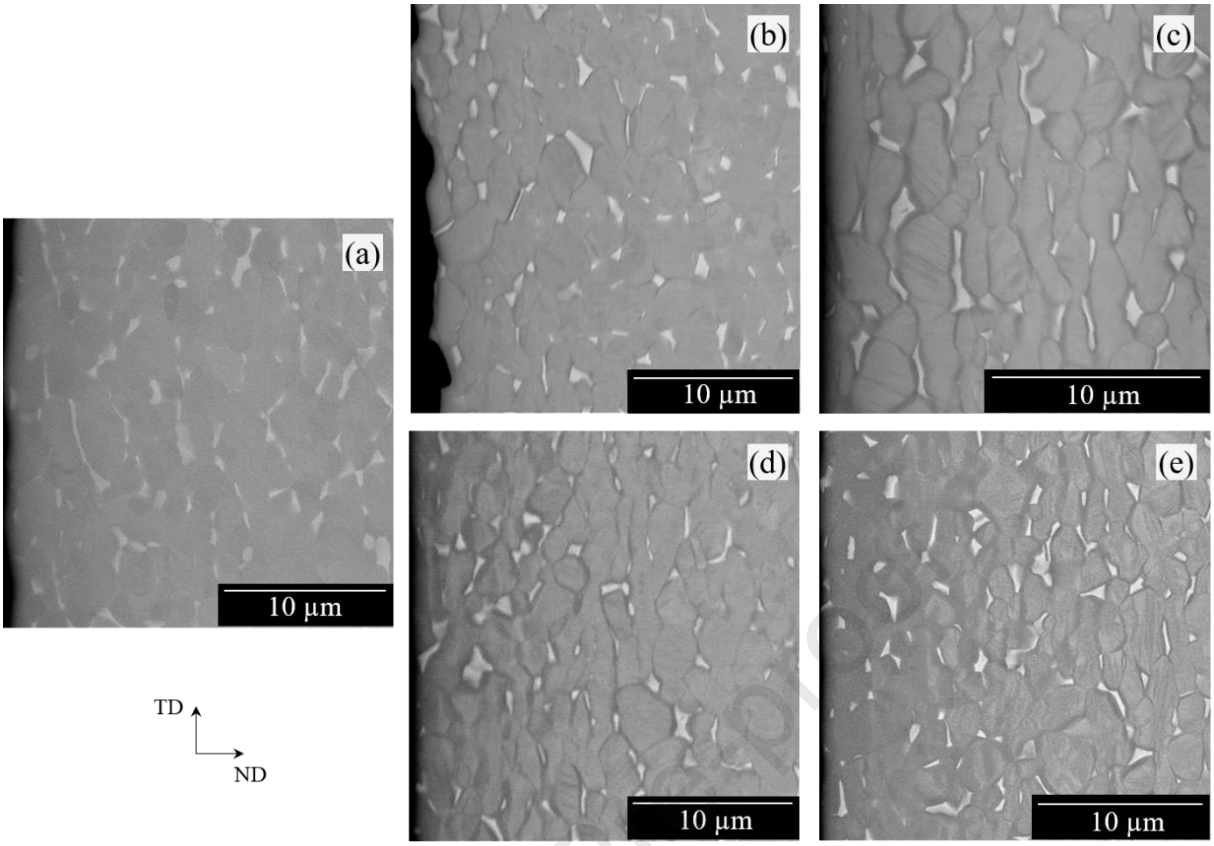

Figure 5: SEM-BSE micrographs on cross sections of hydrogen charged Ti-6Al-4V (cf. Figure 1). Electrochemical hydrogen charging at room temperature for (a) one day at 0.8 mA·cm^{-2}, (b) one week at 0.8 mA·cm^{-2}, (c) three weeks at 0.8 mA·cm^{-2}, (d) one day at 100 mA·cm^{-2}, (e) one day at 200 mA·cm^{-2}. The dark grey colour represents titanium hydrides formed by electrochemical hydrogen charging. Hydride formation increased at phase and grain boundaries in the Ti-α phase upon higher hydrogen charging duration and/or higher charging current densities.

Finally, EBSD scans confirmed the presence of the titanium hydride phase. Figure 6 shows the cross section at 25 µm depth from the edge of a hydrogen charged specimen for 1 day at 200 mA·cm^{-2}. Hydrides were mainly present at phase and grain boundaries. Following the XRD-results, only γ-hydrides were characterised. In order to determine further orientation relationships, Figure 7 shows the corresponding inverse pole figures and pole figures of specific crystallographic directions with respect to the reference system. The titanium hydrides tend to follow only the $\{0001\}_{\text{Ti-}\alpha}$ // $\{001\}_{\text{TiH}\gamma}$ orientation relationship during formation. As elaborated in the discussion, the pole figures match the pattern for prismatic transformation from hexagonal Ti-α into tetragonal γ-hydride.

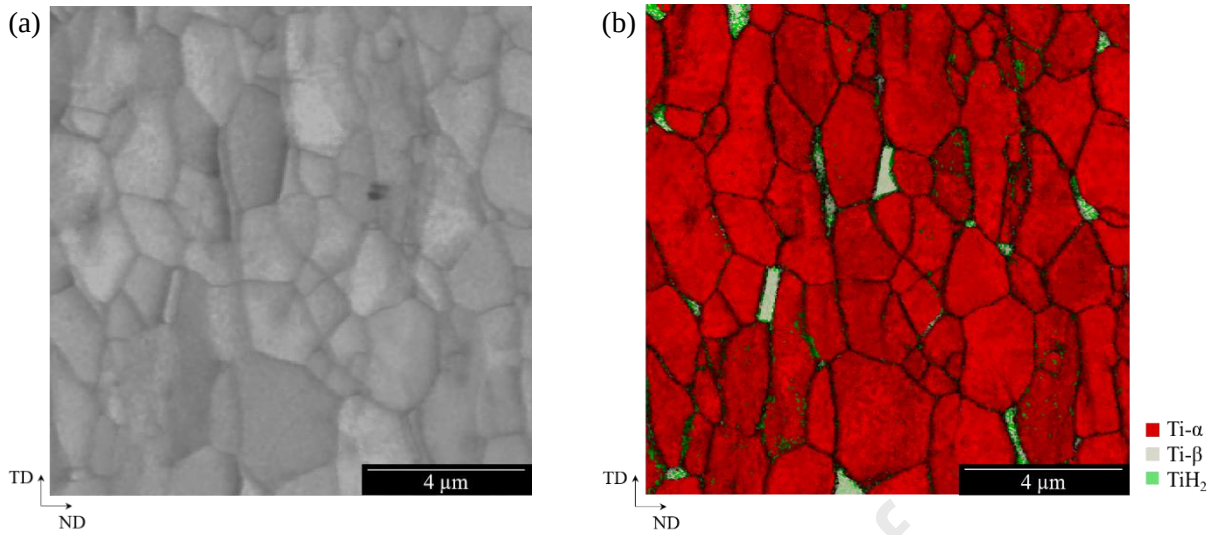

Figure 6: EBSD analysis of cross section of electrochemically hydrogen charged Ti-6Al-4V for 1 day at 200 mA·cm^{-2}, taken at 25 µm depth from the edge. (a) Image quality map. (b) Phase map. The grey γ titanium hydride phase develops preferentially at phase and grain boundaries.

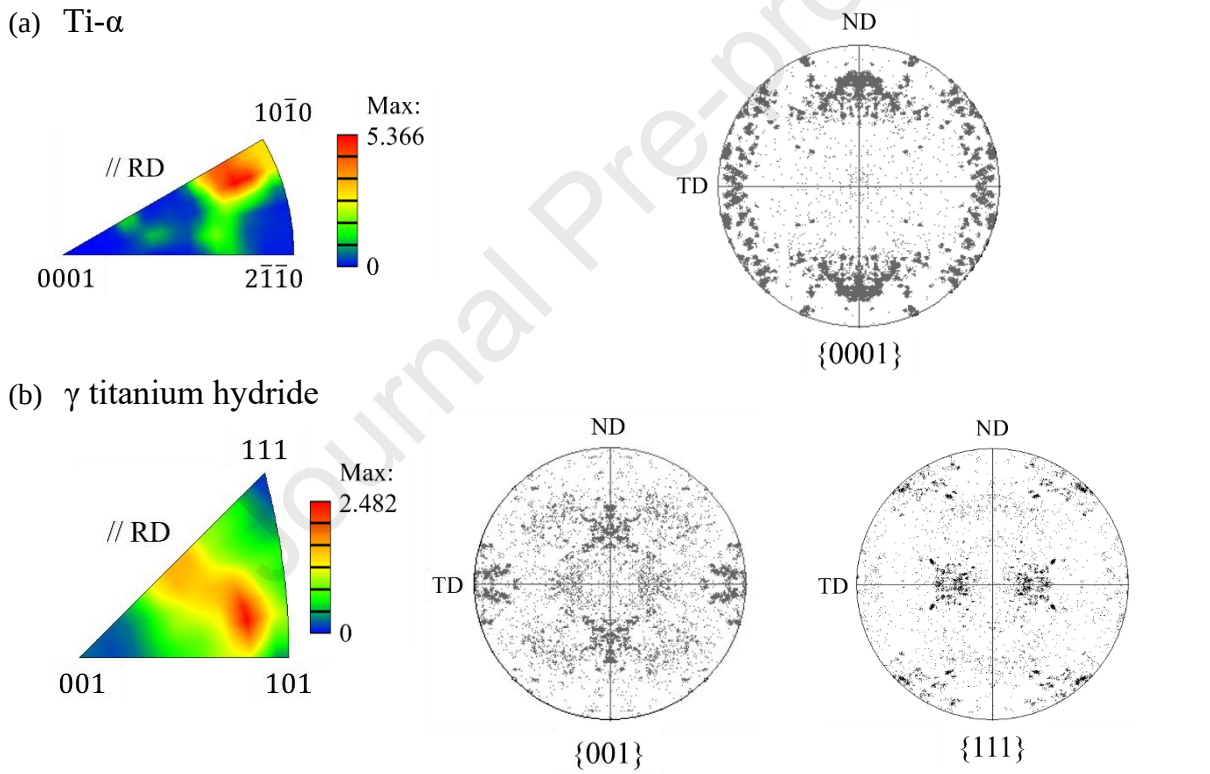

Figure 7: EBSD inverse pole figure and pole figure(s) of (a) Ti-α phase and (b) γ-hydrides after electrochemical hydrogen charging of Ti-6Al-4V for 1 day at 200 mA·cm^{-2}. An orientation relationship between $\{0001\}_{Ti\text{-}\alpha}$ // $\{001\}_{TiH\gamma}$ *is observed.*

4. Discussion

4.1. Hydrogen diffusion in Ti-6Al-4V

Solute hydrogen atoms diffused a deeper distance into the bulk than visible in Figure 5, since hydrides formed locally once a sufficiently high hydrogen concentration was reached. The specific hydrogen diffusion characteristics are discussed below. During galvanostatic hydrogen charging, protons reduce at the titanium's surface. Subsequently, the formed hydrogen atoms are absorbed in the metal. Solving Fick's second law for one dimensional diffusion in a semi-infinite plate, a theoretical hydrogen diffusion profile could be estimated with Equation 1, based on models described by Crank [32]. In this formula, c(x,t) represents the hydrogen concentration at a specific location in the specimen, c_0 the initial hydrogen concentration in the specimen, c_s the hydrogen concentration in the hydrogen supplying electrolyte, x the depth [m], D the diffusion coefficient [$m^2 \cdot s^{-1}$], and t the time [s]. The initial and boundary conditions were considered to be $c=c_0$ for $x>0$ at $t=0$ and $c=c_s$ for $x<0$ at $t=0$-86400, i.e. abundant hydrogen supply during charging, while assuming axial symmetry.

$$c(x,t) = c_0 + c_s \cdot \left(1 - \mathrm{erf}\left(\frac{x}{\sqrt{4Dt}}\right)\right) \qquad \text{Equation 1}$$

The diffusion of hydrogen in Ti-6Al-4V after one day charging at 200 $mA \cdot cm^{-2}$ at room temperature in the considered electrolyte is visualised in Figure 8. A general diffusion coefficient of 10^{-14} $m^2 \cdot s^{-1}$ was used. Here, only hydrogen introduced by charging was considered. It was assumed that the hydrogen present after the production process was homogeneously distributed over the specimen, since the production process occurred at high temperatures where the hydrogen diffusion rate is several orders of magnitude higher. The hydrogen solubility limit in Ti-α, determined from Baker et al. [14], is indicated in the figure by the horizontal threshold line. Above this limit [14], titanium hydrides were formed, hence located in a region close to the edge. Below this threshold, slightly deeper towards the bulk, solid solution hydrogen was present. Meanwhile, the increase of lattice parameter *'c'* in the Ti-α phase upon charging, as indicated by the XRD results in Figure 4 and Table 2, was caused by this interstitial hydrogen. No introduced hydrogen was present near the specimen's centre due to the low hydrogen diffusivity at room temperature.

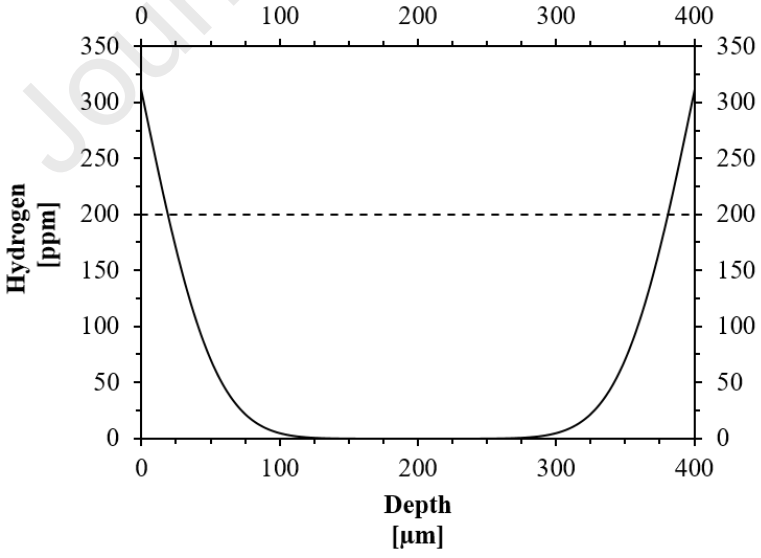

Figure 8: Theoretical charged hydrogen diffusion profile in Ti-6Al-4V specimen with 0.4 mm thickness after one day electrochemical hydrogen charging at 200 mA·cm^{-2}. The dashed line indicates the hydrogen solubility limit in Ti-α, above which, titanium hydrides are likely to form, i.e. nearby the specimen's edges. Below this threshold concentration, solid solution hydrogen is present in the metal.

The increased lattice parameter and XRD peak shift upon charging implied that hydrogen induced uniform lattice expansion and local strains upon penetrating the metal's crystal lattice. Generally,

hydrogen prefers to occupy the tetrahedral interstitial sites in transition metals such as titanium [18]. Also after the formation of titanium hydrides, the Ti-α lattice remained widened. Thus, it can be deduced that solute hydrogen accumulated in the microstructure until the concentration exceeded the threshold for titanium hydride formation in Ti-α. Comparable lattice parameters were reported by Tal-Gutelmacher and Eliezer [12]. However, Kim et al. [33, 34] observed with *in situ* XRD a slightly different trend regarding the lattice constants after hydrogen charging. They described that the Ti-α phase expanded by the introduced hydrogen, analogously predominantly for parameter *'c'*. Besides, a lattice expansion was also claimed to occur in the interconnected Ti-β phase. The dissimilarity compared to the present work could be explained by the different microstructural arrangement, i.e. interconnected Ti-β vs. separated Ti-β islands here, which resulted in dissimilar hydrogen diffusion characteristics. Besides, the lack of lattice parameter increase in the Ti-β phase after charging could also be explained by the fact that the bcc crystal structure is better able to accommodate hydrogen atoms than the hcp phase due to the higher amount of interstitial spots and the lower lattice misfit when hydrogen resides in these interstitial spots [35].

4.2. Effect of hydrogen charging duration and charging current density

The charging parameters and resulting change in microstructure affect the material's interaction with hydrogen. As elaborated in the introduction, the hydrogen diffusion rate in titanium hydride was reported to be higher than in Ti-α and lower than in Ti-β [7, 11, 17]. Hein et al. [36] showed that the hydrogen diffusion coefficient in titanium hydride decreased upon increasing hydrogen content in the stoichiometric formula TiH_x. Thus, initially, the rate limiting factor for hydrogen diffusion in the duplex alloy is hydrogen diffusion in the Ti-α phase. Therefore, the optimal parameters for hydrogen charging duration and current density depend on the application purpose. High current density electrochemical charging for a short duration generated a higher hydrogen content compared to longer charging at low current density. Correspondingly, the titanium hydride quantity at high current density charging was significantly higher than for long duration charging. High current density electrochemical hydrogen charging forced more hydrogen atoms to enter the metal in a short period of time. Combined with the slow diffusion rate, most of the hydrogen remained located close to the edge. Thus, local hydrogen supersaturation occurred early, resulting in titanium hydride formation. Therefore, thin foils with high surface-to-volume ratios are recommended when hydride formation at room temperature is the purpose.

On the other hand, at low charging current density during longer periods, hydrogen was able to diffuse and dissipate into the bulk, without immediately reaching the threshold concentration required for the formation of titanium hydride. Solid solution hydrogen had the chance to spread out in the lattice without achieving bulk hydrogen saturation. The accumulated hydrogen in the Ti-β phase eventually exceeded the solubility limit of the Ti-α phase and formed first titanium hydride at the α-β interface (as elaborated further in paragraph 4.3). Practical feasibility should be considered for these long duration hydrogenations in industrial applications. Meanwhile, titanium demonstrated a certain degree of tolerance against cathodic polarisation conditions, especially at low current densities. Furthermore, a controlled introduction of interstitial hydrogen and titanium hydrides could support the investigation of the different hydrogen assisted failure mechanisms in titanium. Specifically, the respective share in the mechanisms of hydrogen enhanced localised plasticity and stress induced hydride formation [37] are of interest for follow up studies on the hydrogen induced mechanical degradation of these metals.

The common standards for structural titanium alloys require the hydrogen concentration to remain below 150 atomic ppm [21]. The maximal total hydrogen content valued up to 59.1 atomic ppm for a current density of 200 $mA \cdot cm^{-2}$ in the considered 0.4 mm thick specimen. Moreover, no hydrogen induced damage was observed in titanium when subjected to the considered charging parameters, i.e. when one of the charging variables was kept low. Kim et al. [34] also used a comparable diluted sulfuric acid solution at 0.5 $mA \cdot cm^{-2}$ for 40 hours without reporting hydrogen associated damage, while observing titanium hydride formation in a microstructure with interconnected Ti-β. No hydrogen blister formation was observed, whereas it was the case in certain steel alloys under the considered conditions [38]. Furthermore, since only a moderate amount of hydrides developed at the specimen's edge when

minimising one of the charging parameters, no effect of spallation or cracking was seen linked to the volume expansion associated with hydride formation. Alternatively, crack formation was observed during electrochemical charging in another electrolyte consisting of 2/3 vol% glycerol and 1/3 vol% phosphoric acid after 48 hours at 50 mA·cm^{-2} in [39]. Still, both the latter as well as the currently used H_2SO_4 solution abundantly provided protons to facilitate the hydrogen uptake reaction. Therefore, taking all considerations above into account, the current experimental methodology could be considered as a reliable procedure to charge Ti-6Al-4V with hydrogen.

4.3. Hydride formation in Ti-6Al-4V

Next up, the hydride formation characteristics were analysed. When titanium became locally saturated with hydrogen at the specimen's edges, titanium hydrides formed. The hydride formation depth was defined as the deepest distance into the bulk where titanium hydrides were detected. An average of this hydride formation depth taken from three different specimens, is represented in Figure 9. The experimental observations were in line with the theoretical hydrogen diffusion profile of Figure 8. Titanium hydrides were formed in the region close to the edge where the hydrogen solubility of Ti-α was locally exceeded. Furthermore, both for increasing charging duration as well as for increasing current density, the titanium hydride formation depth initially developed quasi linear as a function of the varied charging parameter. For higher current density, however, the rate of the hydride formation depth decreased, which was in line with Hein et al. [36] who reported a decreasing hydrogen diffusion for increasing hydrogen quantity. This transition point was not yet reached for the long duration charging at low current density since hydrogen had in this case more chance to dissipate into the bulk. Nevertheless, more hydrogen present still implied more and deeper hydride formation since the hydrogen solubility limit was exceeded more frequently.

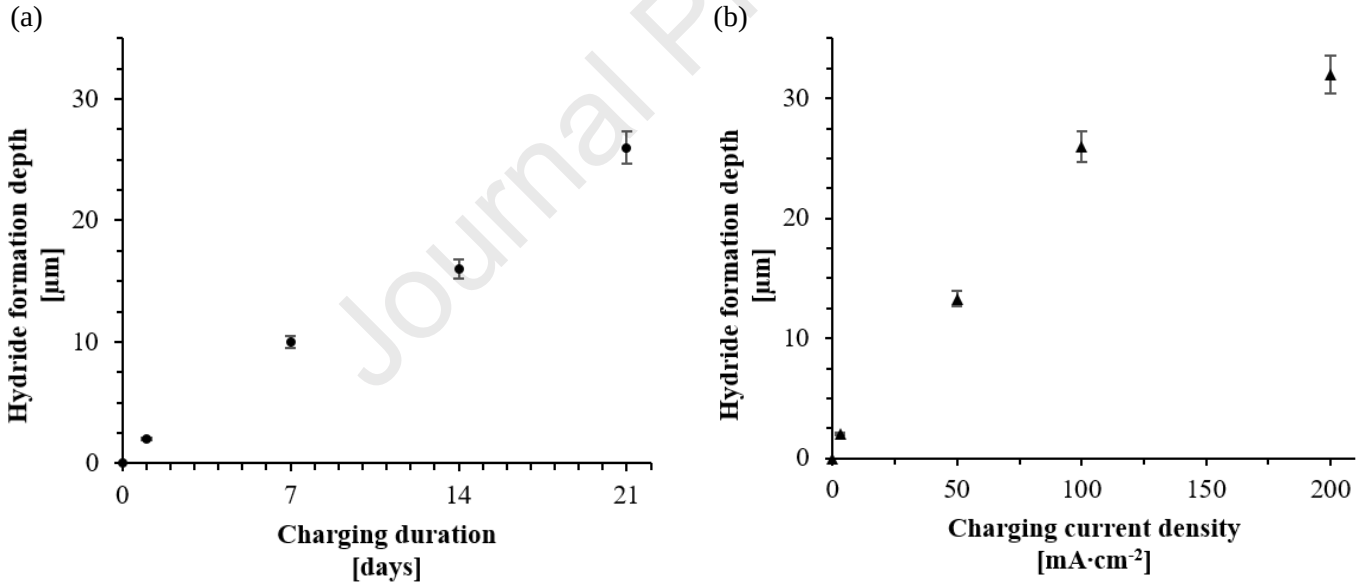

Figure 9: Hydride formation depth into the cross section (a) for multiple charging durations at 0.8 mA·cm^{-2} and (b) for one day of charging at different current densities. The average furthest distance from the edge where titanium hydrides were detected, is reported.

For both parameter variations, only γ-hydrides were formed under these conditions. Kim et al. [34] also observed this fct hydride to appear initially under similar charging conditions at room temperature. Meanwhile, δ-hydrides are rather observed at higher hydrogen concentrations, higher stress concentrations and/or higher temperatures [40]. The hydride formation process was characterised more in depth by SEM-BSE in Figure 10. Depending on the distance from the sample's edge, the progress in the hydride formation mechanism could be estimated. Hydrogen did not reach the centre of the specimen due to the slow diffusion rate of hydrogen in titanium at room temperature. Meanwhile, the high hydrogen concentration at the sample's edge resulted in titanium hydride formation. This gradual transition enabled to identify the subsequent stages of the hydride formation process throughout the

thickness of the specimen. The different zones could be distinguished from the micrographs in Figure 10. Poloni et al. [41] observed a similar evolution during hydrogen charging of Ti-6Al-4V in artificial seawater. Starting in the bulk (zone I), the hydrogen concentration was low. No hydrides were present, while only solid solution hydrogen diffused here. Little closer towards the specimen's surface in zone II, the hydrogen content increased and titanium hydrides nucleated at phase boundaries. Here, the accumulated hydrogen in Ti-β exceeded the hydrogen solubility limit at the interface with Ti-α. Consecutively, with increasing hydrogen content, titanium hydrides developed as well at grain boundaries, as illustrated in Figure 6. In zone III, containing an even higher hydrogen content, the Ti-α grains became supersaturated and started precipitating as titanium hydride laths in Figure 10b. This observation was supported by the peak broadening in the XRD spectra in Figure 4. The TiH_x peaks showed a broad appearance, which could be associated with the scattering of the small size of coherently diffracting domains from developed hydrides together with dislocation scattering. Moreover, the broadening of the Ti-α phase upon hydrogenation was linked to the formation of hydride laths inside the grain, reducing the effective size of coherently diffracting Ti-α domain. Besides, Feaugas et al. [15] explained that hydrogen diffusion has anisotropic characteristics in the hexagonal lattice. The hydrogen diffusion was reported to be faster along the a-axis as a result of the dissimilar packing factors in the planes. Therefore, an intergranular difference was observed in preferential hydride formation orientation. Conforto et al. [42] listed favourable orientation relationships with optimal coherence between the hexagonal substrate and the hydride precipitates. From the EBSD pole figures (Figure 7), the present orientation relationships were comparable to the hydride interaction in pure α titanium. Mainly the prismatic transformation (P-type) from the Ti-α phase into the γ-hydride phase was observed with the characteristic habit plane $\{0001\}_{\text{Ti-}\alpha}$ // $\{001\}_{\text{TiHx}}$ $\langle 1\bar{2}10\rangle_{\text{Ti-}\alpha}$ // $\langle 110\rangle$ $_{\text{TiHx}}$ and interface plane $\{10\bar{1}0\}_{\text{Ti-}\alpha}$ // $\{1\bar{1}0\}_{\text{TiHx}}$ [43]. Transformation via this prismatic habit plane is the result of plane strain transformation, according to Woo et al. [44]. Numakura and Koiwa [45] observed similar lamellae of γ-hydride with TEM in pure titanium. Conforto and Caillard [16] proposed that the γ-hydrides nucleate in prismatic planes at the low energy interface plane in this orientation relationship. When the amount of hydrogen excessively increases, the γ-hydride will transform into δ-hydride. Finally, in Figure 10, all Ti-α grains transformed into titanium hydride due to the high hydrogen concentration at the sample's edge in zone IV. Since the Ti-β phase is able to dissolve more hydrogen than Ti-α, the Ti-β phase did not transform into titanium hydride. Even after extreme charging conditions, e.g. charging for 3 weeks at 200 $mA \cdot cm^{-2}$, islands of the Ti-β phase remained present in the titanium hydride layer as visible in Figure 11. Microcracks were present in the outer hydride layer in order to accommodate the stresses associated with the volume expansion of the phase transformation.

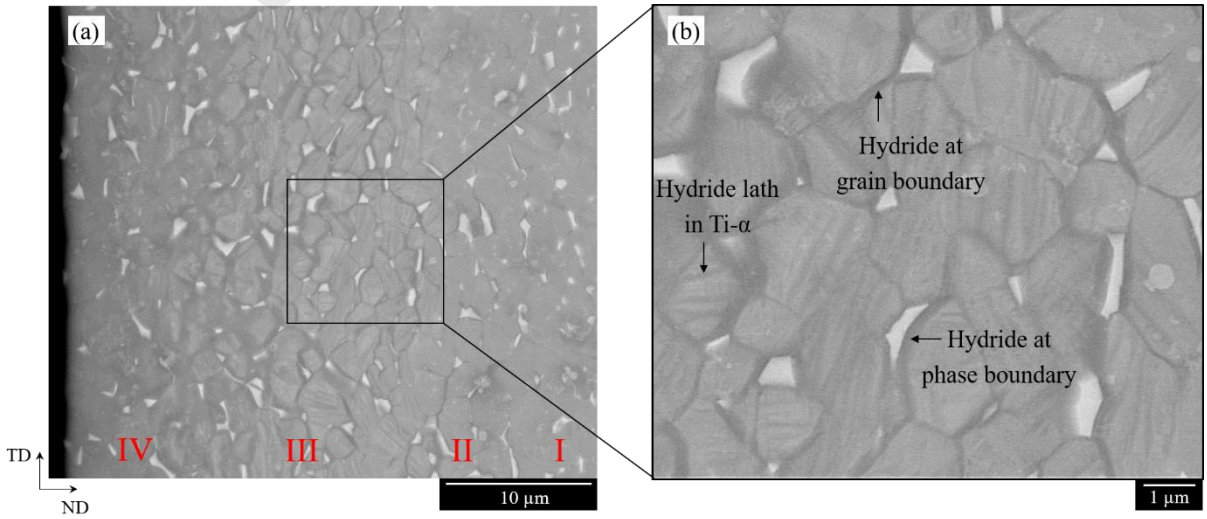

Figure 10: Ti-6Al-4V cross section after 24 hours of charging at 200 $mA \cdot cm^{-2}$. (a) Multiple stages of hydride development are differentiated. I: Solute hydrogen is present in the bulk material consisting of Ti-α and Ti-β phase. II: Titanium hydrides nucleate and grow locally at phase boundaries, and subsequently also at grain boundaries.

III: Quasi-parallel titanium hydride laths form across Ti-α grains upon local hydrogen supersaturation. IV: All Ti-α grains are transformed into titanium hydride, while Ti-β remains intact. (b) Close-up of titanium hydrides at the phase and grain interfaces with the development of hydride laths inside the Ti-α phase.

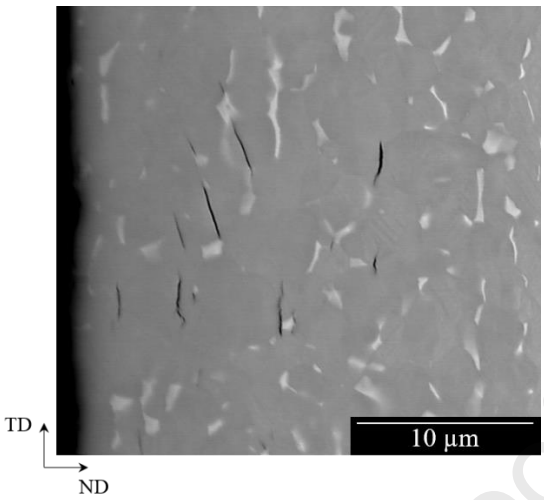

Figure 11: Ti-6Al-4V cross section after 3 weeks of charging at 200 mA·cm^{-2}. Islands of Ti-β phase were still present in the titanium hydride layer. Microcracks appeared in the developed hydride layer in order to accommodate the stresses associated with the volume expansion of the phase transformation.

The mechanism of progressive hydride formation as a result of the increasing hydrogen penetration is schematically proposed in Figure 12. When charging hydrogen, hydrogen in solid solution diffuses through the metal (Figure 12b). Upon increased charging, hydrogen atoms accumulated at the α-β interfaces since hydrogen atoms have a higher solubility and diffusion rate in Ti-β. Subsequently, titanium hydride precipitated along phase boundaries (Figure 12c) and subsequently at the grain boundaries (Figure 12d), since the hydrogen solubility in Ti-α was exceeded there first. Indeed, the impact of hydrogen depends on the microstructure, as reported by Nelson et al. [7, 46]. These researchers demonstrated that the presence of the Ti-β phase attracted hydrogen in a higher quantity than Ti-α tolerated [46]. Since the Ti-β phase was not continuous in the present work, also grain boundaries served as important hydrogen transport paths for faster hydrogen diffusion because of the atomic mismatch. Zeng et al. [47] reported the diffusion coefficient of hydrogen along the grain boundaries of commercially pure titanium at room temperature to be $9.1 \cdot 10^{-9}$ $m^2 \cdot s^{-1}$, which is several orders of magnitude faster than hydrogen diffusion through the Ti-α grain and presumably even faster than hydrogen diffusion in the Ti-β phase. Upon increasing hydrogen concentration, titanium hydrides nucleated in the supersaturated α-grain as hydride laths (Figure 12e, cf. Figure 10b). The enhanced energy due to lattice distortion was minimised by segregation of Ti-α in hydrogen-rich hydride laths and hydrogen-lean Ti-α zones with lower distortion by hydrogen, similar to observations by Shan et al. [23]. Lath formation typically occurred according to a favourable grain orientation, depending on the matrix texture, as reported by Wang et al. in commercially pure titanium [43]. They demonstrated that titanium hydrides form in the crystal direction that is able to relax the largest expansion misfit from the hydride transition. As such, the hydride region gradually expanded at the expense of the Ti-α phase. Meanwhile, Ti-β did not become saturated and maintained its structure (Figure 12g). Eventually, upon particularly high hydrogen concentrations, microcracks developed in the titanium hydride layer (Figure 12h). The volume expansion associated with the phase transformation is the evident cause of the damage [7]. Tal-Gutelmacher and Eliezer claimed that such cracks are typically present inside the primary Ti-α grains [39]. Current observations showed all categories of cracks, interphasal and transphasal, as well as intergranular and transgranular cracking. Taking into account the three dimensionality of a crack, it could have initiated at specific locations, and propagated further along the weakest path. Thus, this overall mechanism explains the non-uniform hydride formation during high fugacity hydrogen charging at room temperature.

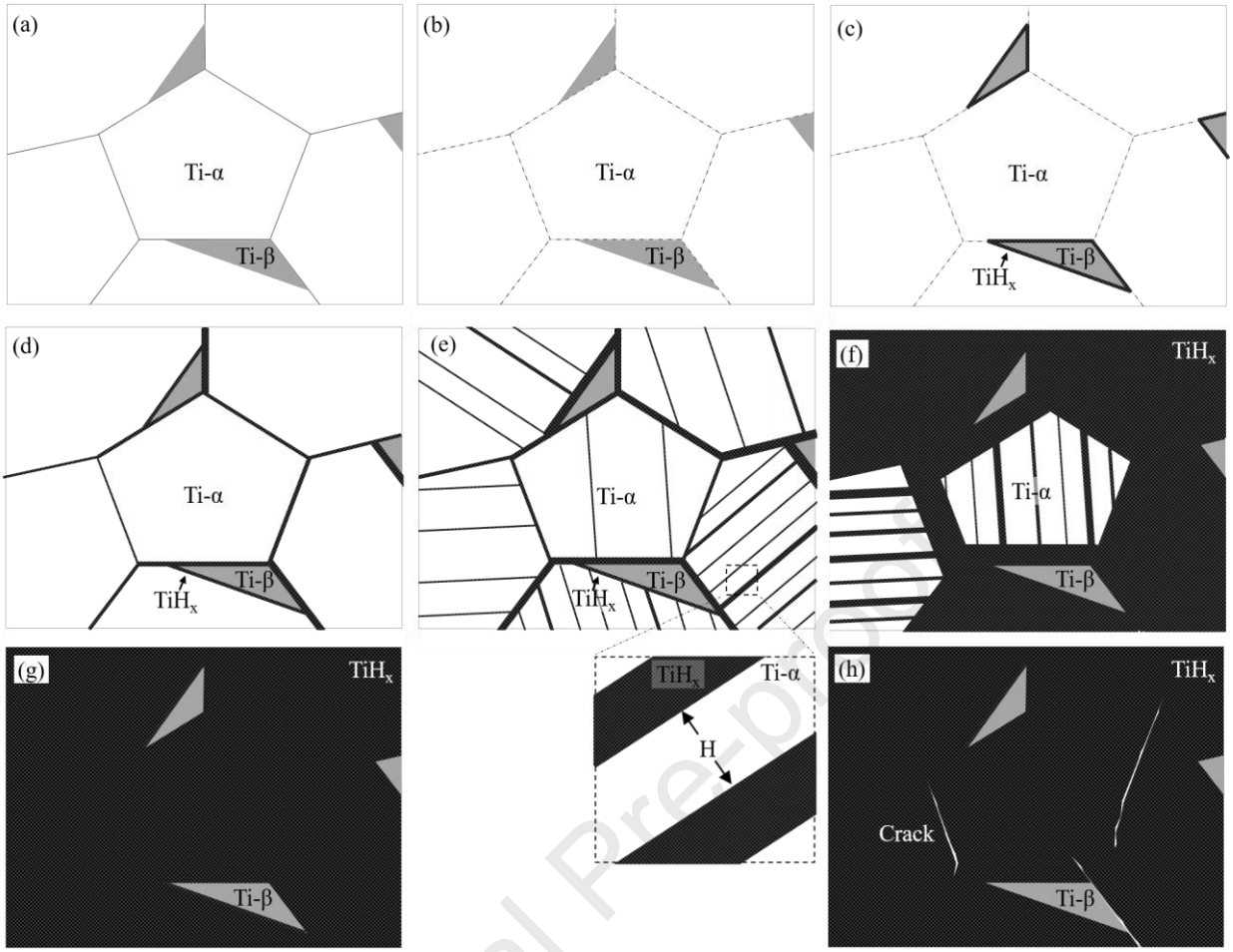

Figure 12: Schematic representation of the mechanism of hydride formation in Ti-6Al-4V under electrochemical hydrogen charging at room temperature. (a) Ti-6Al-4V duplex microstructure with Ti-β islands in the Ti-α matrix. (b) In the first stage, solid solution hydrogen diffuses through the lattice. Hydrogen resides especially in the Ti-β phase and along grain boundaries, respectively due to the high hydrogen solubility and the lattice distortion. (c) Titanium hydrides nucleate at phase boundaries since the hydrogen solubility in Ti-α is locally exceeded. (d) With increasing hydrogen content, hydrides also precipitate along grain boundaries, an important hydrogen transport path. (e) Titanium hydride laths form across Ti-α grains. The dotted frame represents a close-up of local hydrogen diffusion from hydrogen-lean Ti-α to hydrogen-rich titanium hydride laths. (f) Ti-α grains transform fully into titanium hydride. (g) Due to the higher hydrogen solubility in Ti-β, this phase coexists in the titanium hydride matrix. (h) Upon high hydrogen charging, transgranular and intergranular microcracks develop in the microstructure to accommodate the high stresses linked to the volume expansion of the phase transformation.

5. Conclusion

The mechanism of hydride formation in duplex Ti-6Al-4V microstructure during electrochemical hydrogen charging at room temperature was identified and discussed. The effect of charging duration and current density were analysed.

- Titanium hydride formation under these conditions was a non-uniform process, starting at the sample surface in contact with the electrolyte. At low hydrogen concentration, hydrogen diffused as solid solution interstitial element in the lattice, resulting in lattice strains. At higher hydrogen concentration, titanium hydrides nucleated first at the phase and grain boundaries.
- Upon hydrogen supersaturation of the α-grain, titanium hydride laths precipitated. With increasing hydrogen content, Ti-α completely transformed into titanium hydride, mainly according to the prismatic transformation type. The Ti-β phase remained unaffected since the hydrogen solubility limit was not exceeded there.
- The applied charging current density showed a major effect on the hydrogen content with subsequent hydride formation due to faster hydrogen introduction in the material. Contrarily, long charging at low current density formed less hydrides as hydrogen dissipated more into the material.
- Under extreme hydrogen charging, microcracks formed in the hydride layer to accommodate the stresses associated with the phase transformation. However, no microstructural damage was created when keeping either charging duration or current density low. Therefore, these controllable hydrogen charging conditions provide opportunities for investigation of hydrogen induced failure, thermohydrogen processing, etc.

CRediT authorship contribution statement

L. Deconinck: Conceptualisation, Methodology, Validation, Investigation, Formal analysis, Visualisation, Writing – original draft. **T. Depover**: Conceptualisation, Methodology, Writing – Review & Editing, Supervision, Project administration, Funding acquisition. **K. Verbeken**: Methodology, Writing – Review & Editing, Supervision, Project administration, Funding acquisition

Declaration of competing interest

The authors declare that they have no known competing financial interests or personal relationships that could have appeared to influence the work reported in this paper.

Data availability

The raw/processed data required to reproduce these findings cannot be shared at this time as the data also forms part of an ongoing study.

Acknowledgements

The authors wish to acknowledge the support of the Flanders Research Foundation for the senior postdoctoral fellowship (FWO grant 12ZO420N) as well as the Ghent University Special Research Fund (grant BOF15/BAS/062 and BOF20/BAS/121).

References

[1] A. Gulyaev, *Physical Metallurgy*. MIR Publishers, 1980.

[2] C. R. Brooks, *Heat Treatment, Structure and Properties of Nonferrous Alloys*. ASM International, 1982.

[3] G. Lütjering and J. C. Williams, *Titanium*, 2nd ed. Berlin: Springer, 2007. doi: 10.1007/978-3-540-73036-1.

[4] E. Tal-Gutelmacher and D. Eliezer, "Hydrogen-Assisted Degradation of Titanium Based Alloys," *Mater. Trans.*, vol. 45, no. 5, pp. 1594–1600, 2004, doi: 10.2320/matertrans.45.1594.

[5] J. Bellosta von Colbe, J.-R. Ares, J. Barale, M. Baricco, C. Buckley, G. Capurso, N. Gallandat, D. M. Grant, M. N. Guzik, I. Jacob, E. H. Jensen, T. Jensen, J. Jepsen, T. Klassen, M. V Lototskyy, K. Manickam, … M. Dornheim, "Application of hydrides in hydrogen storage and compression: Achievements, outlook and perspectives," *Int. J. Hydrogen Energy*, vol. 44, pp. 7780–7808, 2019, doi: 10.1016/j.ijhydene.2019.01.104.

[6] O. N. Senkov and F. H. Froes, "Thermohydrogen processing of titanium alloys," *Int. J. Hydrogen Energy*, vol. 24, pp. 565–576, 1999, doi: doi.org/10.1016/S0360-3199(98)00112-8.

[7] H. G. Nelson, "Hydrogen Embrittlement," in *Treatise on Materials Science and Technology*, vol. 25, Academic Press, 1983, pp. 275–359. doi: 10.1016/b978-0-12-341825-8.50014-3.

[8] Y. Chang, A. J. Breen, Z. Tarzimoghadam, P. Kürnsteiner, H. Gardner, A. Ackerman, A. Radecka, P. A. J. Bagot, W. Lu, T. Li, E. A. Jägle, M. Herbig, L. T. Stephenson, M. P. Moody, D. Rugg, D. Dye, … B. Gault, "Characterizing solute hydrogen and hydrides in pure and alloyed titanium at the atomic scale," *Acta Mater.*, vol. 150, pp. 273–280, 2018, doi: 10.1016/j.actamat.2018.02.064.

[9] A. San-Martin and F. D. Manchester, "The H-Ti (Hydrogen-Titanium) system," *Bull. Alloy Phase Diagrams*, vol. 8, no. 1, pp. 30–42, 1987, doi: 10.1007/BF02868888.

[10] F. H. Froes, O. N. Senkov, and J. I. Qazi, "Hydrogen as a temporary alloying element in titanium alloys: thermohydrogen processing," *Int. Mater. Rev.*, vol. 49, no. 3–4, pp. 227–245, 2004, doi: 10.1179/095066004225010550.

[11] L. Luo, Y. Su, J. Guo, and H. Fu, "Formation of titanium hydride in Ti-6Al-4V alloy," *J. Alloys Compd.*, vol. 425, pp. 140–144, 2006, doi: 10.1016/j.jallcom.2006.01.014.

[12] E. Tal-Gutelmacher and D. Eliezer, "The hydrogen embrittlement of titanium-based alloys," *J. Mater.*, vol. 57, no. 9, pp. 46–49, 2005, doi: 10.1007/s11837-005-0115-0.

[13] E. Tal-Gutelmacher, D. Eliezer, and D. Eylon, "The effects of low fugacity hydrogen in duplex- and beta-annealed Ti-6Al-4V alloy," *Mater. Sci. Eng. A*, vol. 381, pp. 230–236, 2004, doi: 10.1016/j.msea.2004.04.020.

[14] H. Baker, Ed., *Alloy Phase Diagrams*, 10th ed. ASM International, 1992.

[15] X. Feaugas and E. Conforto, "Influence de l'hydrogène sur les mécanismes de déformation et d'endommagement des alliages de titane et de zirconium," *PlastOx 2007 - Mec. Mec. des Interact. Plast. - Environ.*, vol. 2007, pp. 161–178, 2009, doi: 10.1051/ptox/2009012.

[16] E. Conforto and D. Caillard, "A fast method for determining favourable orientation relationships and interface planes: Application to titanium-titanium hydrides transformations," *Acta Mater.*, vol. 55, no. 3, pp. 785–798, 2007, doi: 10.1016/j.actamat.2006.06.061.

[17] O. Ivasishin and V. Moxson, "Low-cost titanium hydride powder metallurgy," in *Titanium powder metallurgy: Science, Technology and Applications*, Butterworth-Heinemann, 2015, pp. 117–148. doi: 10.1016/B978-0-12-800054-0.00008-3.

[18] H. Wipf, B. Kappesser, and R. Werner, "Hydrogen diffusion in titanium and zirconium hydrides," *J. Alloys Compd.*, vol. 310, pp. 190–195, 2000, doi: 10.1016/S0925-8388(00)00945-2.

[19] C. Yexin, "Kinetics of Hydrogen Diffusion in Ti-6Al-4V Alloy," *Rare Met. Mater. Eng.*, vol. 44, no. 3, pp. 553–556, 2015, doi: 10.1016/S1875-5372(15)30037-0.

[20] C. L. Briant, Z. F. Wang, and N. Chollocoop, "Hydrogen embrittlement of commercial purity titanium," *Corros. Sci.*, vol. 44, pp. 1875–1888, 2002, doi: 10.1016/S0010-938X(01)00159-7.

[21] P. Sun, Z. Z. Fang, M. Koopman, J. Paramore, and K. S. R. Chandran, "An experimental study of the (Ti-6Al-4V)-xH phase diagram using in situ synchrotron XRD and TGA/DSC techniques," *Acta Mater.*, vol. 84, pp. 29–41, 2015, doi: 10.1016/j.actamat.2014.10.045.

[22] F. H. Froes, D. Eliezer, O. N. Senkov, and J. I. Qazi, "Beneficial effects of hydrogen as a temporary alloying element in titanium alloys: An overview," *Hydrog. Eff. Mater. Behav. Corros. Deform. Interact. - Proc. Int. Conf. Hydrog. Eff. Mater. Behav. Corros. Deform. Interact.*, pp. 301–313, 2003.

[23] D. B. Shan, Y. Y. Zong, T. F. Lu, and Y. Lv, "Microstructural evolution and formation mechanism of FCC titanium hydride in Ti-6Al-4V-xH alloys," *J. Alloys Compd.*, vol. 427, pp. 229–234, 2007, doi: 10.1016/j.jallcom.2006.02.058.

[24] H. J. Liu, L. Zhou, P. Liu, and Q. W. Liu, "Microstructural evolution and hydride precipitation mechanism in hydrogenated Ti-6Al-4V alloy," *Int. J. Hydrogen Energy*, vol. 34, no. 23, pp. 9596–9602, 2009, doi: 10.1016/j.ijhydene.2009.09.098.

[25] H. Z. Xiao, "On the mechanism of hydride formation in α-Ti alloys," *Scr. Metall. Mater.*, vol. 27, no. 5, pp. 571–576, 1992.

[26] ASTM International, "ASTM B265, Standard Specification for Titanium and Titanium Alloy Strip, Sheet and Plate." West Conshohocken, 2020.

[27] S. Liu, Z. Zhang, J. Xia, and Y. Chen, "Effect of Hydrogen Precharging on Mechanical and Electrochemical Properties of Pure Titanium," *Adv. Eng. Mater.*, vol. 22, no. 5, pp. 1–11, 2020, doi: 10.1002/adem.201901182.

[28] P. Metalnikov, D. Eliezer, and G. Ben-Hamu, "Hydrogen trapping in additive manufactured Ti-6Al-4V alloy," *Mater. Sci. Eng. A*, vol. 811, p. 141050, 2021, doi: 10.1016/j.msea.2021.141050.

[29] H. R. Z. Sandim, B. V. Morante, and P. A. Suzuki, "Kinetics of Thermal Decomposition of Titanium Hydride Powder Using in situ High-temperature X-ray Diffraction (HTXRD)," *Mater. Res.*, vol. 8, no. 3, pp. 293–297, 2005, doi: 10.1590/S1516-14392005000300012.

[30] H. Yan, J. Kim, and C. C. Tasan, "In-situ scanning electron microscope thermal desorption spectroscopy (SEM-TDS) analysis of thermally-induced titanium hydride decomposition and reformation," *Acta Mater.*, vol. 226, p. 117562, 2022, doi: 10.1016/j.actamat.2021.117562.

[31] L. G. Paratt, "Surface Studies of Solids by Total Reflection of X-Rays," *Phys. Rev.*, vol. 95, no. 2, pp. 359–369, 1954, doi: 10.1103/physrev.95.359.

[32] J. Crank, *The mathematics of diffusion*. Oxford: Clarendon Press, 1975.

[33] J. Kim, E. Plancher, and C. C. Tasan, "Hydrogenation-induced lattice expansion and its effects on hydrogen diffusion and damage in Ti-6Al-4V," *Acta Mater.*, vol. 188, pp. 686–696, 2020, doi: 10.1016/j.actamat.2020.02.029.

[34] J. Kim, J. Kang, and C. C. Tasan, "Hydride formation in Ti6Al4V: An in situ synchrotron X-ray diffraction study," *Scr. Mater.*, vol. 193, pp. 12–16, 2021, doi: 10.1016/j.scriptamat.2020.10.025.

[35] T. P. Chapman, D. Dye, and D. Rugg, "Hydrogen in Ti and Zr alloys: industrial perspective , failure modes and mechanistic understanding," *Philos. Trans. A*, vol. 375, p. 20160418, 2017,

doi: 10.1098/rsta.2016.0418.

[36] M. Hein, A. Bals, A. F. Privalov, and H. Wipf, "Gorsky effect study of H and D diffusion in V and Ti at high H(D) concentrations," *J. Alloys Compd.*, vol. 356–357, pp. 318–321, 2003, doi: 10.1016/S0925-8388(03)00111-7.

[37] D. S. Shih, I. M. Robertson, and H. K. Birnbaum, "Hydrogen embrittlement of α titanium: In situ tem studies," *Acta Metall.*, vol. 36, no. 1, pp. 111–124, 1988, doi: 10.1016/0001-6160(88)90032-6.

[38] A. Laureys, E. Van den Eeckhout, R. Petrov, and K. Verbeken, "Effect of deformation and charging conditions on crack and blister formation during electrochemical hydrogen charging," *Acta Mater.*, vol. 127, pp. 192–202, 2017, doi: 10.1016/j.actamat.2017.01.013.

[39] E. Tal-Gutelmacher and D. Eliezer, "High fugacity hydrogen effects at room temperature in titanium based alloys," *J. Alloys Compd.*, vol. 406, pp. 613–616, 2005, doi: 10.1016/j.jallcom.2004.12.172.

[40] E. Conforto and X. Feaugas, "A Review of Hydride Precipitates in Titanium and Zirconium Alloys: Precipitation, Dissolution and Crystallographic Orientation Relationships," *MATEC Web Conf.*, vol. 321, p. 11042, 2020, doi: 10.1051/matecconf/202032111042.

[41] A. Poloni, A. Oudriss, J. Creus, C. Berziou, E. Conforto, C. Saval, S. Frappart, T. Millot, A. Mathis, and X. Feaugas, "Hydrogen absorption and hydride formation in pure titanium T40 (grade 2) and TA6V ELI (grade 23) under cathodic polarization in artificial seawater," *MATEC Web Conf.*, vol. 321, p. 09006, 2020, doi: 10.1051/matecconf/202032109006.

[42] E. Conforto, S. Cohendoz, C. Berziou, P. Girault, and X. Feaugas, "Formation and dissolution of hydride precipitates in zirconium alloys: Crystallographic orientation relationships and stability after temperature cycling," *Mater. Sci. Forum*, vol. 879, pp. 2330–2335, 2017, doi: 10.4028/www.scientific.net/MSF.879.2330.

[43] Q. Wang, S. Xu, J.-S. Lecomte, C. Schuman, L. Peltier, X. Shen, and W. Song, "Crystallographic orientation dependence of hydride precipitation in commercial pure titanium," *Acta Mater.*, vol. 183, pp. 329–339, 2020, doi: 10.1016/j.actamat.2019.11.027.

[44] T. Woo, G. C. Weatherlyt, C. E. Coleman, and R. W. Gilbert, "The precipitation of y-deuterides (hydrides) in titanium," *Acta Metall.*, vol. 33, no. 10, pp. 1897–1906, 1985.

[45] H. Numakura and M. Koiwa, "Hydride precipitation in Titanium," *Acta Metall.*, vol. 32, no. 10, pp. 1799–1807, 1984.

[46] H. G. Nelson, D. P. Williams, and J. E. Stein, "Environmental hydrogen embrittlement of an α-β titanium alloy: Effect of microstructure," *Metall. Trans.*, vol. 3, no. 2, pp. 473–479, 1972, doi: 10.1007/BF02642051.

[47] Y. Zeng, J. J. Noël, P. R. Norton, and D. W. Shoesmith, "Hydrogen transport through thin titanium oxides," *J. Electroanal. Chem.*, vol. 649, pp. 277–285, 2010, doi: 10.1016/j.jelechem.2010.06.022.

The mechanism of hydride formation during electrochemical hydrogen charging of Ti-6Al-4V

Authors: L. Deconinck, T. Depover*, K. Verbeken*

Highlights

- Controlled formation of hydrides in Ti-6Al-4V by electrochemical hydrogen charging
- Charging current density determines hydride formation more than charging duration
- Detailed formation mechanism of titanium hydrides upon hydrogen supersaturation

Declaration of interests

☒ The authors declare that they have no known competing financial interests or personal relationships that could have appeared to influence the work reported in this paper.

☐ The authors declare the following financial interests/personal relationships which may be considered as potential competing interests: